JOURNAL OF THE AMERICAN CHEMICAL SOCIETY

Article

pubs.acs.org/JACS

Ion Dynamics in Porous Carbon Electrodes in Supercapacitors Using in Situ Infrared Spectroelectrochemistry

Francis W. Richey,[†] Boris Dyatkin,[‡,§] Yury Gogotsi,[‡,§] and Yossef A. Elabd*[,†]

[†]Department of Chemical and Biological Engineering, [‡]A.J. Drexel Nanotechnology Institute, and [§]Department of Materials Science and Engineering, Drexel University, Philadelphia, Pennsylvania 19104, United States

Ⓢ *Supporting Information*

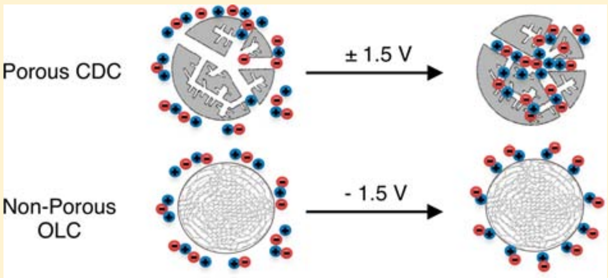

ABSTRACT: Electrochemical double layer capacitors (EDLCs), or supercapacitors, rely on electrosorption of ions by porous carbon electrodes and offer a higher power and a longer cyclic lifetime compared to batteries. Ionic liquid (IL) electrolytes can broaden the operating voltage window and increase the energy density of EDLCs. Herein, we present direct measurements of the ion dynamics of 1-ethyl-3-methylimidazolium bis((trifluoromethyl)sulfonyl)imide in an operating EDLC with electrodes composed of porous nanosized carbide-derived carbons (CDCs) and nonporous onion-like carbons (OLCs) with the use of in situ infrared spectroelectrochemistry. For CDC electrodes, IL ions (both cations and anions) were directly observed entering and exiting CDC nanopores during charging and discharging of the EDLC. Conversely, for OLC electrodes, IL ions were observed in close proximity to the OLC surface without any change in the bulk electrolyte concentration during charging and discharging of the EDLC. This provides experimental evidence that charge is stored on the surface of OLCs in OLC EDLCs without long-range ion transport through the bulk electrode. In addition, for CDC EDLCs with mixed electrolytes of IL and propylene carbonate (PC), the IL ions were observed entering and exiting CDC nanopores, while PC entrance into the nanopores was IL concentration dependent. This work provides direct experimental confirmation of EDLC charging mechanisms that previously were restricted to computational simulations and theories. The experimental measurements presented here also provide deep insights into the molecular level transport of IL ions in EDLC electrodes that will impact the design of the electrode materials' structure for electrical energy storage.

INTRODUCTION

Electrochemical double layer capacitors (EDLCs), also referred to as supercapacitors, are energy storage devices offering exceptionally large power densities that can be used to harvest energy produced by intermittent renewable energy sources.[1] Given the square dependence of the energy density on applied voltage windows for EDLCs, a key strategy to enhance charge storage capacity is to implement electrolytes and electrolyte/electrode combinations with higher electrochemical stabilities. Room temperature ionic liquids (ILs) are promising electrolyte alternatives, due to their larger voltage windows, low flammability, and large operating temperature ranges (−50 to +150 °C).[2,3] Although ILs possess favorable properties for use as electrolytes in EDLCs, the double layer structure and molecular level ion dynamics of IL electrolytes are still not well understood.[4,5] In addition to understanding the dynamics of ILs during the formation of a charge-storing electric double layer, it is important to differentiate the behavior for ion confinement in endohedral porous structures and open charge mobility around exohedral nonporous particles.[6] For traditional supercapacitors, carbide-derived carbons (CDCs), produced via halogen etching of metal carbides, have offered important advantages, including high surface areas (in excess of 1000 m^2/g) and tunable pore structures that depend on the carbide precursor and synthesis conditions.[7] In supercapacitor configurations with matching ion and pore diameters, molecular simulations predict desolvation of ions and resulting superionic state high-density ion packing in pores.[8,9] Despite these molecular predictions, direct experimental evidence of this phenomenon is limited, and the dynamics of ion transport through hierarchical branched pore networks are not fully understood. Conversely, onion-like carbons (OLCs) exhibit lower surface areas (and lower resulting gravimetric capacitance), but allow for much higher power densities due to diminished diffusion limitations.[10] Given the spherical nature of these particles, molecular simulations[11] have attempted to explain the effects of curvature and resulting differences in the double layer structure (as compared to the flat electrode surface carbon allotropes, such as CDC or graphene). However, direct experimental evidence is needed to fully explain these effects.

A deeper understanding of the charging/discharging behavior of ILs in EDLCs with porous CDC and nonporous OLC particles will require molecular level in situ experimental techniques. Molecular dynamics simulations have recently shown that both cations and anions of ILs occupy the pores

Received: June 18, 2013
Published: August 5, 2013

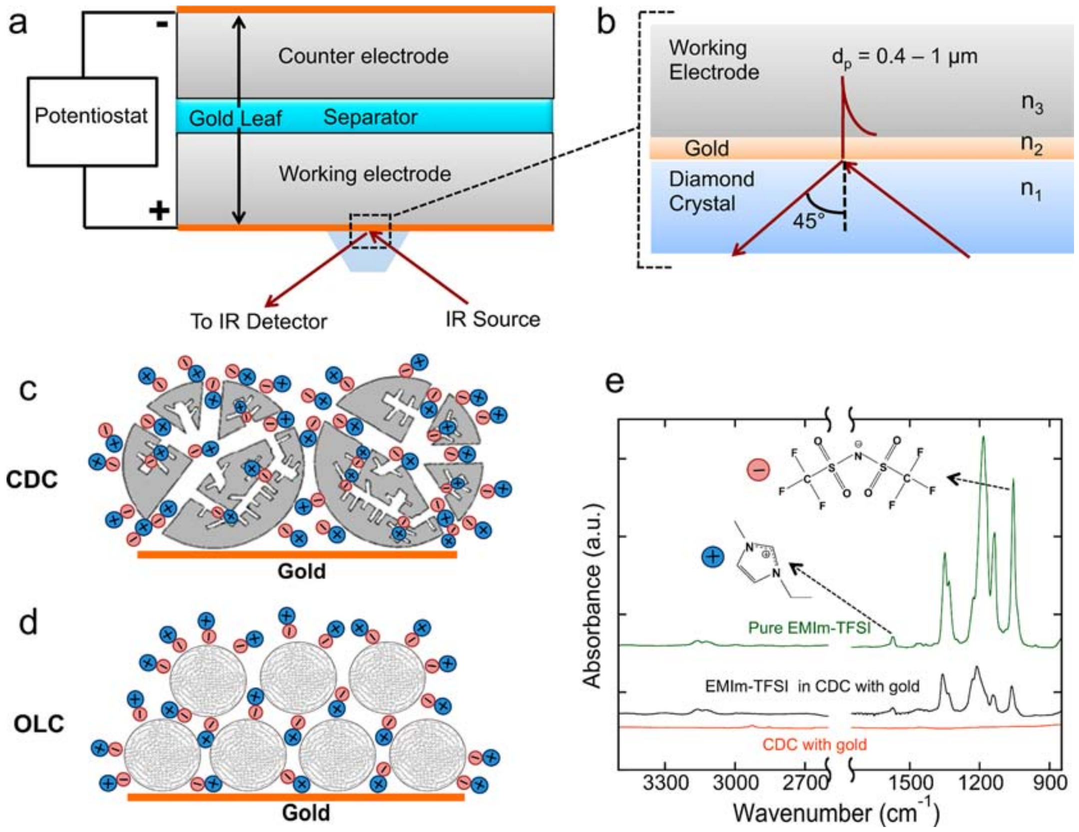

Figure 1. (a) Schematic of the spectroelectrochemical experiment with the supercapacitor on the ATR crystal of the FTIR spectrometer and (b) magnified view of the crystal/electrode interface showing the sampling depth into the working electrode in the range of 0.4−1 μm. (c, d) Illustration of ions in electrodes consisting of porous CDC particles and exohedral OLC particles on a gold current collector. (e) Infrared spectra of pure EMIm-TFSI (no gold) and CDC on gold with and without EMIm-TFSI.

of the carbon particles in EDLCs under both negative and positive applied potential.[12] Unfortunately, there are only a few in situ experimental techniques capable of measuring ion dynamics in carbon electrodes of EDLCs, including NMR spectroscopy[13] and electrochemical quartz crystal microbalance,[14,15] neither of which have been used to study ILs as the electrolyte. In this work, we present results on the ion dynamics of an IL on the molecular level in EDLC electrodes using an in situ infrared spectroelectrochemical technique recently developed in our laboratory.[16] More specifically, results will be shown for IL (1-ethyl-3-methylimidazolium bis((trifluoromethyl)sulfonyl)imide (EMIm-TFSI)) ion dynamics in the electrodes of an entire functioning EDLC, where the electrodes are composed of OLCs, as well as nanosized CDCs. Spectroelectrochemical techniques similar to the one presented here that combine standard electrochemical measurements with in situ infrared spectroscopy (i.e., infrared spectroelectrochemistry) are useful for studying EDLCs, because of their ability to couple chemical changes with electrical inputs/outputs.[17,18] Infrared spectroelectrochemistry that utilizes attenuated total reflectance (ATR) has been used to study fuel cell electrodes[19,20] and corrosion processes,[21] but requires the fragile ATR crystal to be modified and typically cannot examine an entire working device. The technique developed for this work allows us to examine multiple functioning EDLCs without modifying the ATR crystal surface. Herein, in situ infrared spectroelectrochemistry is employed for the first time to measure direct molecular level chemical changes in EDLC electrodes as a function of voltage. The measurements provide a fundamental understanding of the differences in charging rates and mechanisms between porous (CDC) and dense spherical (OLC) carbon particles.

■ RESULTS

Figure 1a shows a cross-sectional schematic of the EDLC on the ATR crystal of the infrared spectrometer. The EDLC consists of symmetric 75 μm thick electrodes composed of carbon particles, poly(tetrafluoroethylene) (PTFE) binder (10 wt %), and EMIm-TFSI separated by a Celgard membrane. Both CDC particles with endohedral pores (Figure 1c) and exohedral nonporous OLC particles (Figure 1d) were used as the active materials in the electrodes; see the Supporting Information (Figure S1) for Brunauer−Emmett−Teller (BET) analysis of both carbon materials. The gold film (~60 nm) on the electrode surface serves as a current collector during spectroelectrochemical experiments. Figure 1b shows an enlarged schematic of the crystal/electrode interface. The optical system shown in Figure 1b consists of three phases, each with their own respective refractive index; n_1, n_2, and n_3 correspond to the diamond ATR crystal, gold current collector, and carbon working electrode, respectively. The solution to the three-phase optical system presented here has been previously presented by Hansen et al.[22] The depth of penetration, d_p, or sampling depth, is defined in the following equation as the distance into the working electrode for which the electric field produced by the incident light decreases by a factor of $1/e$:

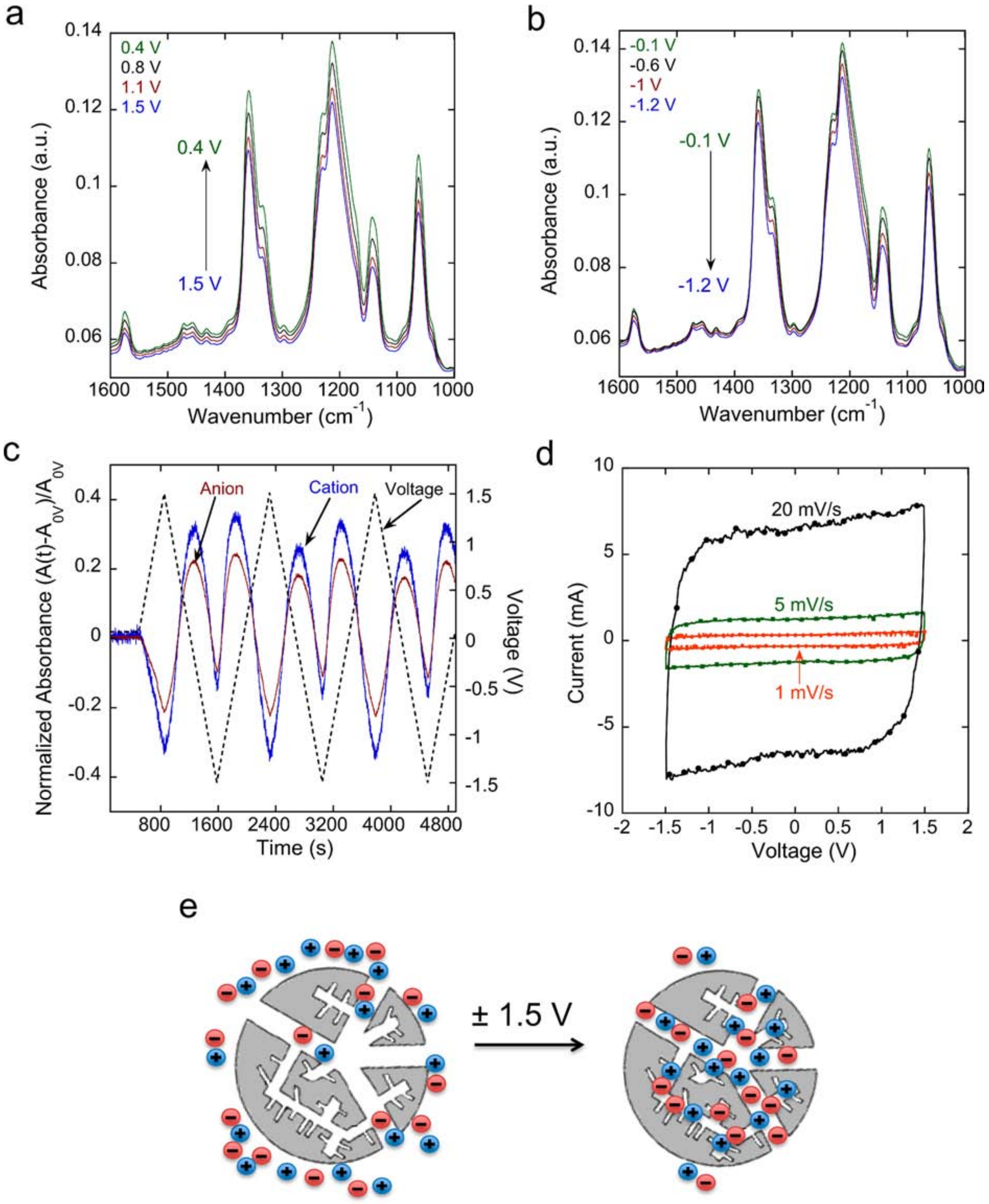

Figure 2. Results for CDC electrodes: time-resolved infrared spectra corresponding to (a) positive and (b) negative voltages during a CV scan from −1.5 to +1.5 V; (c) normalized absorbance of the infrared bands of the cation and anion of EMIm-TFSI as a function of time during three CV cycles from −1.5 to +1.5 V at a scan rate of 5 mV/s (open circuit voltage (OCV) 0.068 V); (d) corresponding CV scans at three different scan rates; (e) schematic illustrating the ion dynamics within pores of CDC particles during CV experiments.

$$d_{\mathrm{p}} = \frac{\lambda_0}{4\pi \ \mathrm{Im} \sqrt{{n_3}^2 - {n_1}^2 \sin^2 \theta}} \tag{1}$$

In eq 1, λ_0 is the wavelength of light, n_3 is the refractive index of the carbon working electrode with EMIm-TFSI, n_1 is the refractive index of the diamond ATR crystal, θ is the angle of incident light, and Im refers to the imaginary part of the square root.[22] d_{p} varies with the wavelength from 0.4 to 1 μm (see the Supporting Information for the calculation). With a known sampling depth (d_{p}), the volume of the electrode sampled is ~0.001 mm^3 (0.008% of the total electrode volume), which corresponds to 2 × 10^8 carbon particles (see the Supporting Information for the calculation). Therefore, although a small volume of the electrode is sampled, the total number of particles probed is significantly large due to the small size of the carbon nanoparticles. As shown in the illustrations in Figure 1c,d, carbon nanoparticles (CDCs and OLCs) create a smooth interface between the working electrode and the gold current collector (see the microscopy results in Figure S1).

Figure 1e shows representative infrared spectra of pure EMIm-TFSI (without gold) and CDC on gold with and without EMIm-TFSI. The spectrum of the pure EMIm-TFSI electrolyte shows sharp infrared absorbance bands representing the chemical bonds in the cation (1575 $\mathrm{cm^{-1}}$, C=C stretch) and the anion (1070 $\mathrm{cm^{-1}}$, SO_2 stretch). For the CDC on gold spectrum, only a few low-intensity infrared absorbance bands are evident in the 2800−3000 $\mathrm{cm^{-1}}$ range and are representative of the C−H stretching in the carbon particles. The CDC on gold with EMIm-TFSI spectrum appears similar to the pure EMIm-TFSI spectrum for several reasons. One reason for this behavior is the porous electrodes absorb over 100% of their weight in EMIm-TFSI due to their large surface area. Strong absorption of infrared light by EMIm-TFSI over a broad wavelength range along with a very weak IR spectrum for carbon allows us to easily monitor the electrolyte spectrum. The thin gold current collector on the electrode surface acts as an optical filter and absorbs a portion of the incident photons;[22] hence, the infrared intensity of the EMIm-TFSI in the electrode is ∼33% smaller than the pure EMIm-TFSI intensity.

Parts a and b of Figure 2 show time-resolved infrared spectra of EMIm-TFSI in the CDC electrode of an operating EDLC in response to changes in the applied potential. The infrared spectra show that intensity is largest when the voltage is close to 0 V and decreases as the voltage moves further from 0 V in the positive or negative direction. These results suggest that the changes in intensity of the EMIm-TFSI absorbance bands are the result of the EMIm-TFSI ions entering or leaving the CDC pores as the EDLC is charged or discharged during a cyclic voltammetry (CV) experiment from −1.5 to +1.5 V. When ions enter the pores of the CDC, they are no longer detected due to the carbon particles blocking the infrared signal; hence, the absorbance decreases as the electrode charges (ions fill pores) and increases as the electrode discharges (ions leave pores). In Figure 2a,b, infrared bands representing both the cation and anion of EMIm-TFSI increase or decrease simultaneously with changes in the voltage. Estimates of ion sizes (EMIm, ∼0.76 nm; TFSI, ∼0.79 nm)[23,24] and the calculated CDC mean pore size (0.85 nm; Figure S1, Supporting Information) suggest chainlike aggregate ion transfer as depicted in Figure 2e and are in agreement with molecular dynamic simulations performed by Merlet et al.[12] showing both cations and anions of an ionic liquid occupying the pores of carbon particles during charging and discharging. The densely packed and strongly interacting ions in EMIm-TFSI do not separate during charging, instead moving as aggregates of ions into the pores to compensate for the changing voltage. We previously observed dynamics of ILs as aggregates in RuO_2 pseudocapacitors,[16] but the data in this work are the first direct measurement of IL ion transfer in pores of particles.

In Figure 2c, the absorbances of the cation and anion bands are plotted versus time over the course of three CV cycles from −1.5 to +1.5 V. The absorbance is initialized and normalized by the absorbance at 0 V, A_{0V}, to compare the change in absorbance between the cation and anion more effectively. Here it should be noted that the change in absorbance of ions adsorbing on the gold current collector is less than 5% of the change in absorbance in the carbon electrodes (see the Supporting Information, Figure S2). In Figure 2c, as the voltage increases from 0 to +1.5 V, the absorbances of both the cation and anion decrease as ions enter the pores of the CDC particles.

When the current changes direction and the voltage is scanned from +1.5 V back to 0 V, the absorbance increases as the ions are expelled from the pores and the absorbance reaches a maximum as the voltage approaches 0 V. Although the current does not change direction at 0 V, the absorbance begins to decrease again as the voltage starts moving away from 0 V in the negative direction (0 to −1.5 V), indicating ions re-entering the pores. Thus, ion sorption in CDC pores seems to be dictated by the voltage rather than the current direction. Conversely, the normalized absorbance profile for IL ions in RuO_2 pseudocapacitors mirrored the direction of the electrical current, which does not change direction at 0 V during CV experiments from +1.5 to −1.5 V due to the nonporous RuO_2 particles and the large concentration of protons present in the Nafion binder.[25] In Figure 2c, as the voltage approaches −1.5 V, the absorbance of both the cation and anion reaches a new minimum as the pores again fill with ions. This same absorbance behavior of the cation and anion is observed for the scan direction from −1.5 to +1.5 V and is repeatable for a large number of CV sweeps. Additionally, the magnitude of the change in absorbance during CV experiments is proportional to the operating voltage window (see the Supporting Information, Figure S3). This is an expected result, as more IL ions should enter the pores to compensate for higher applied voltages.

Figure 2d shows corresponding CVs for different voltage scan rates, where a voltage-dependent current is observed. This agrees with the absorbance data in Figure 2c and can be attributed to additional ions entering the pores of the CDC particles as the voltage increases. The phenomenon of ions entering the pores of the CDC particles during charging is illustrated in Figure 2e. For a typical CV experiment, when the absorbance of the ions is plotted versus the charge, a convex parabolic curve is obtained (see the Supporting Information, Figure S4). The absorbance approaches a maximum when the charge is close to zero and decreases as the charge increases (in either direction) and ions enter the pores of the CDC particles. This behavior is similar to the concave parabolic results obtained when mass is plotted versus charge for in situ electrochemical quartz crystal microbalance experiments on carbon EDLC electrodes.[15] Additionally, when the voltage scan rate increases from 1 to 20 mV/s, the maximum absorbance shifts further away from the OCV as ions cannot enter the pores of the CDC particles fast enough to compensate for the changing voltage (see Figure S4).

Galvanostatic experiments were also performed to examine the rate at which ions enter the pores of the CDC particles (see the Supporting Information, Figure S5). Under constant current conditions, the linear portion of the absorbance versus time curve can be used to calculate an effective diffusion coefficient of 1.2×10^{-10} $\mathrm{m^2/s}$ for the ions entering the CDC pores. The effective diffusion coefficient calculated here is larger than the value reported using single-particle microelectrode techniques,[26,27] but closer to the self-diffusion coefficient of EMIm-TFSI ions, which is reported to be ca. 4×10^{-11} $\mathrm{m^2/s}$.[28] Self-diffusion coefficients are calculated over small length scales, where diffusion is not impeded by the macroscopic environment that ions must transport through in an electrode. Since an effective diffusion coefficient was calculated that is slightly faster than the self-diffusion coefficient, it is implied that the transport

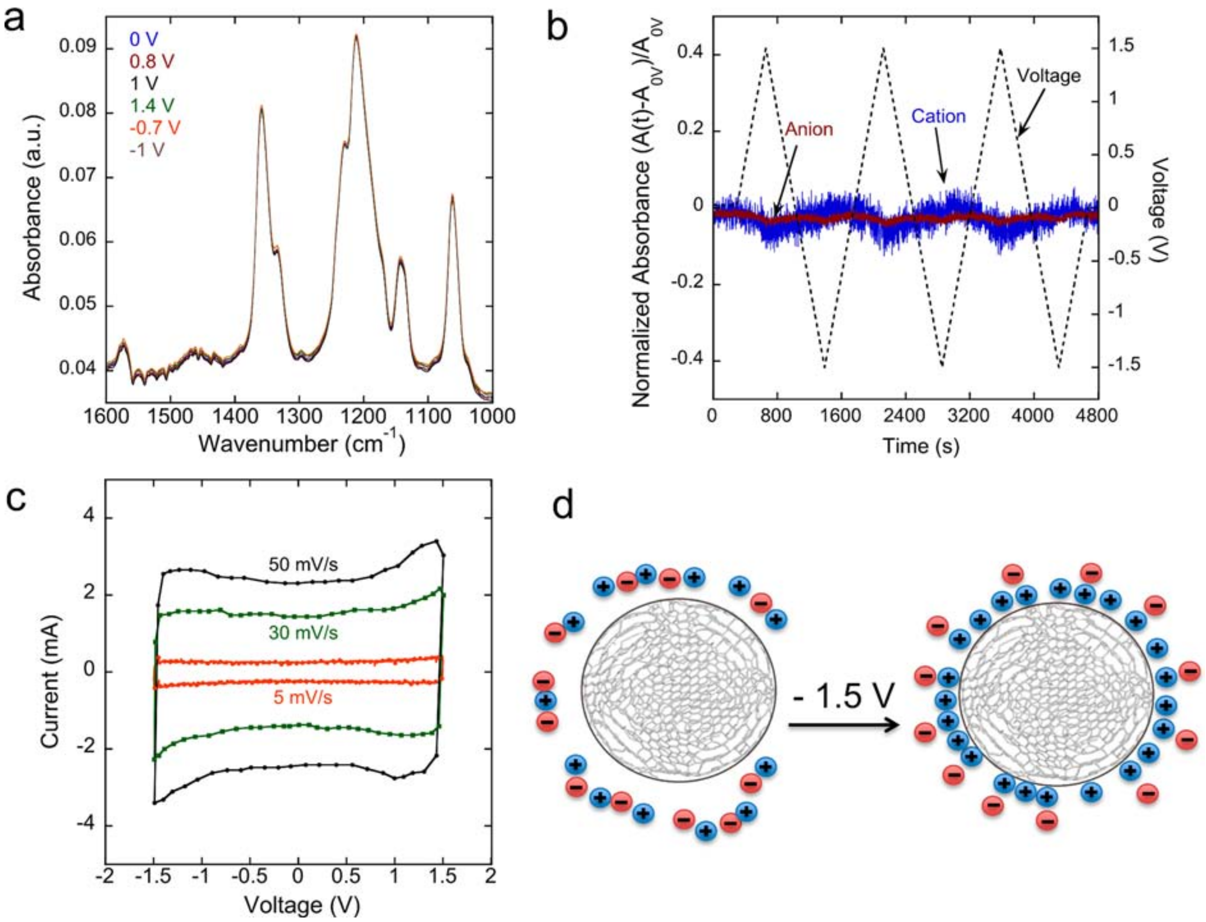

Figure 3. Results for OLC electrodes: (a) time-resolved infrared spectra corresponding to a CV experiment from −1.5 to +1.5 V; (b) normalized absorbance of the infrared bands of the cation and anion of EMIm-TFSI as a function of time during three CV cycles from −1.5 to +1.5 V at 5 mV/s; (c) corresponding CV scans at three different scan rates; (d) schematic illustrating the ion dynamics around OLC particles during CV experiments.

of ions into the pores of CDC particles is also influenced by the environment (interactions with carbon pore walls), capillary forces, and voltage.

Figure 3a shows time-resolved infrared spectra of EMIm-TFSI in an OLC electrode of an operating EDLC at different voltages during a CV sweep from −1.5 to +1.5 V. The spectra of EMIm-TFSI in the electrodes in the charged state (±1 V) and uncharged state (0 V) are nearly identical. In other words, the concentration of ions detected by the spectrometer is nearly unchanged when the OLC electrodes are charged and uncharged. Additionally, there is no shift in any infrared peak position during charging, suggesting that the environment surrounding the ions does not change significantly. This result is in stark contrast to the results obtained for the CDC electrodes, where the differences in the spectra of the charged and uncharged electrodes were clearly visible in Figure 2a,b. When the normalized absorbances of the cation and anion of EMIm-TFSI are plotted versus time, as shown in Figure 3b, the change in absorbance is within the noise of the data; therefore, no statistical change is observed. The change in normalized absorbance of the cation and anion of EMIm-TFSI for the OLC electrodes is less than 10% of the change in absorbance of these ions for the CDC electrodes. This agrees with in situ electrochemical dilatometry results, which show that charging OLC electrodes causes them to swell significantly less than CDC electrodes.[29,30] Since OLCs are nonporous exohedral particles, the ions are predominantly adsorbed on the surface of the OLC particles where they can still be detected by the spectrometer; hence, only a small change in absorbance is expected. Furthermore, the magnitude of the change in absorbance in Figure 3b is similar to that of the change in absorbance for a capacitor without any carbon (only the gold current collectors), and therefore, any change in absorbance in the OLC electrodes is a result of ion adsorption on the surface of the gold current collector and closely positioned OLC particles (see the Supporting Information, Figure S2).

Figure 3c shows CV scans at three different voltage scan rates for the OLC electrodes. Compared to that of the CV scans of the CDC electrodes in Figure 2d, the current for OLC electrodes is ca. 66% smaller. The CV scans of the OLC electrodes do not display the same voltage dependence as was observed for the CDC electrodes, because the charge is stored on the surface of OLCs rather than in the pores of CDCs. Figure 3d illustrates the charging mechanism for OLCs, where the EMIm-TFSI ions are adsorbed on the surface during charging and move away from the surface during discharging, with minimal change in the bulk ion concentration. At the same time, it explains why OLC electrodes can be charged at rates of up to 100 V/s and operate with viscous ionic liquids at −50 °C when long-range transport across the separator membranes is kinetically slow.[3,10] Additionally, the concentration of EMIm-TFSI in the electrodes is significant (ca. 55 wt % EMIm-TFSI), resulting in an excess amount of ions present at the OLC surface. Therefore, the high charging rates of OLCs are a result

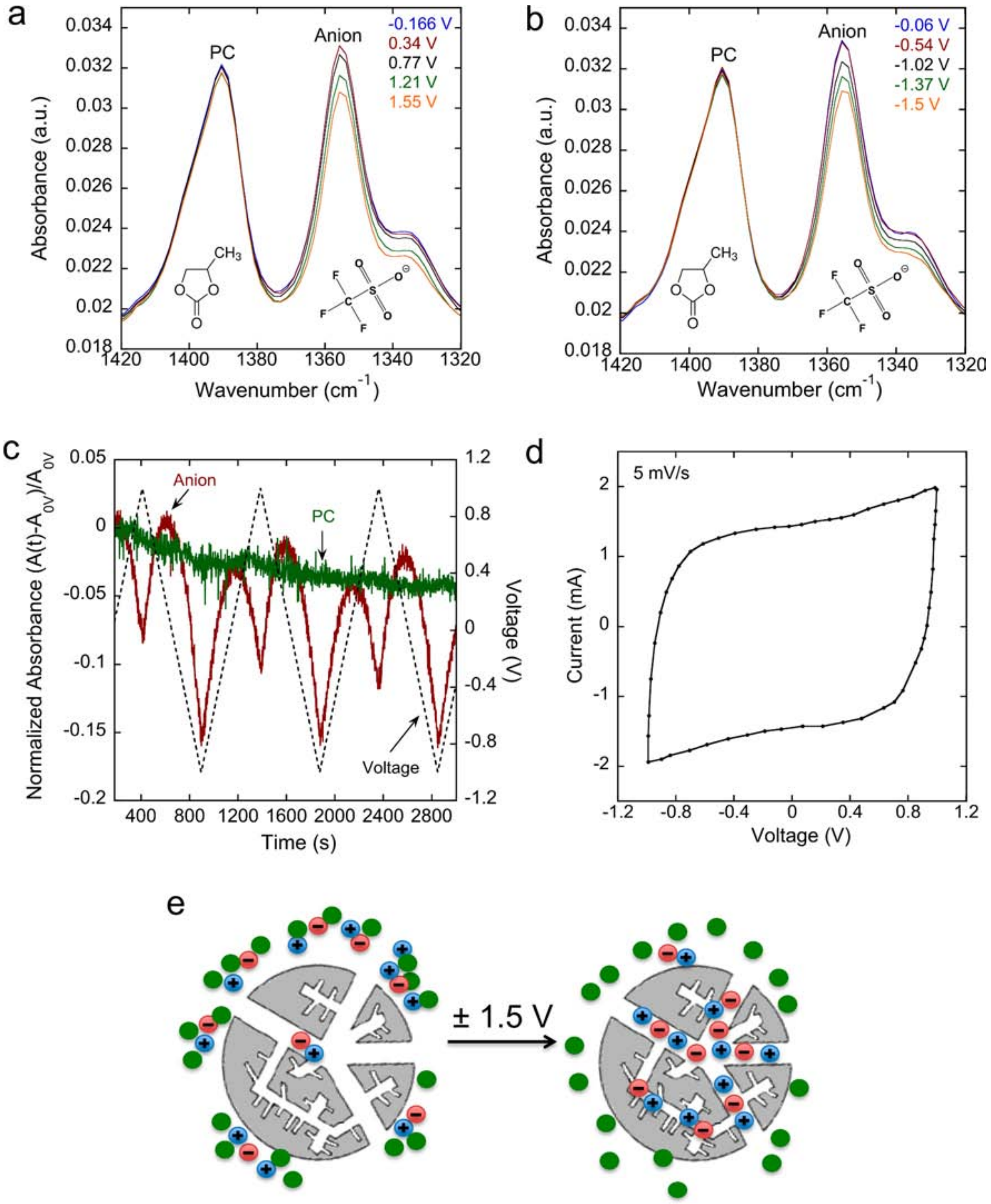

Figure 4. Results for CDC electrodes with a 9:1 mass ratio PC/EMIm-TFSI electrolyte: (a, b) time-resolved infrared spectra corresponding to a CV experiment in the positive and negative voltage ranges, respectively; (c) normalized absorbance of the infrared bands of the anion of EMIm-TFSI (red) and the PC (green) solvent as a function of time during three CV cycles from −1 to +1 V; (d) corresponding CV scans at 5 mV/s; (e) schematic illustrating the ion dynamics into the pores of the CDC, where PC (green circles) does not enter the pores.

of ions within close proximity to the OLCs moving only small distances as they adsorb on the OLC surface as illustrated in Figure 3d. The results presented in Figure 3 show that electrodes with OLCs (or carbon nanotubes[3] and graphene[31]) and ionic liquids can charge at high rates with only a small change in the bulk ionic liquid concentration in the electrode. This is impossible in the case of porous carbon particles because the transport of ions within the pores is kinetically hindered.

Figure 4 shows spectroelectrochemical experiments on CDC electrodes with an electrolyte mixture consisting of a 9:1 mass ratio of propylene carbonate (PC) and EMIm-TFSI. Parts a and b of Figure 4 show time-resolved spectra for the positive and negative voltages of a CV scan, respectively, with only the propylene carbonate (~1390 cm^{-1}) and TFSI anion (~1355 cm^{-1}) bands shown for comparison; see the Supporting Information (Figure S6) for full spectra of pure propylene carbonate, EMIm-TFSI, and the 9:1 mass ratio mixture. The TFSI anion band intensity changes as a function of the voltage

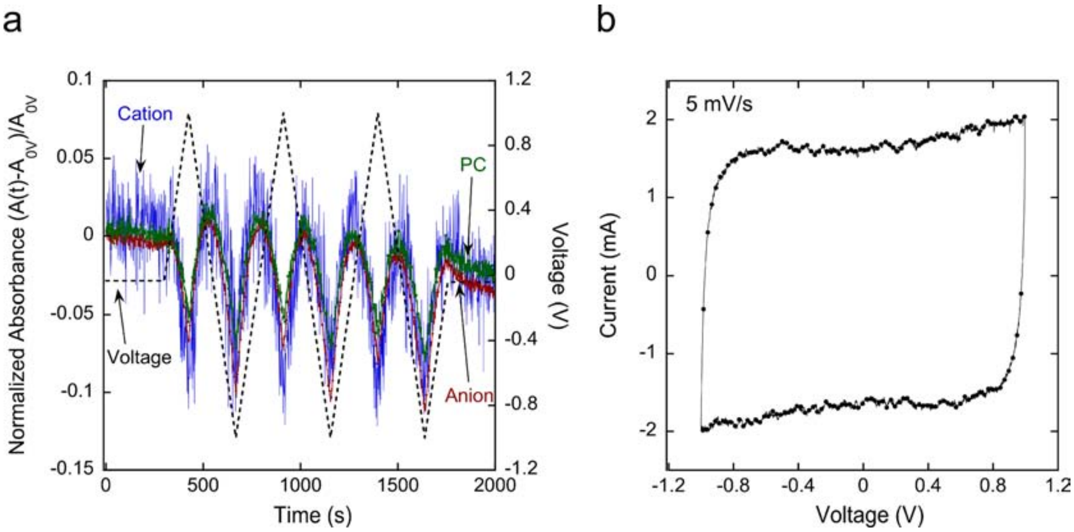

Figure 5. Results for CDC electrodes with a 1:1 mass ratio PC/EMIm-TFSI electrolyte: (a) normalized absorbance of the infrared bands of the anion TFSI (red), cation EMIm (blue), and PC (green) solvent as a function of time during three CV cycles from −1 to +1 V; (b) corresponding CV scans at 5 mV/s.

during charging in both the positive and negative directions, similar to the results in Figure 2 for an electrode with only EMIm-TFSI as the electrolyte. However, the change in the PC infrared band is considerably different. In Figure 4c, the normalized absorbances of the TFSI anion and PC infrared bands are plotted as a function of time over three CV cycles from −1 to +1 V. The normalized absorbance of the PC decreases slightly over the course of the three CV cycles, possibly due to evaporation or small amounts of PC being trapped in the particles. These data show that the TFSI anions are at least partially desolvated when entering the subnanometer pores of the CDC particles during charging. Figure 4d shows the corresponding CV scan at a scan rate of 5 mV/s, where the current is similar to the current for the CDC electrodes in pure EMIm-TFSI (Figure 2d) despite the fact that there are significantly fewer EMIm-TFSI ions in the electrodes with PC/EMIm-TFSI electrolyte (5.87×10^{-6} mol) compared to the electrodes with the pure EMIm-TFSI electrolyte (5.87×10^{-5} mol). These results agree with the work of Gebbie et al.,[32] where they also confirm that only a small fraction of the ions in EMIm-TFSI participate in the charging process, while the majority of the remaining ions behave like neutral aggregates similar to a solvent. Figure 4e illustrates the charging process for the CDC electrode with EMIm-TFSI/PC as the electrolyte, where the desolvated EMIm-TFSI ions enter the pores of the CDC during charging, but the propylene carbonate does not enter the pores.

Figure 5 shows spectroelectrochemical experiments on CDC electrodes with a more concentrated IL electrolyte mixture consisting of a 1:1 mass ratio of PC and EMIm-TFSI, with a concentration similar to that of a conventional organic electrolyte.[33] Similar to Figure 4c, Figure 5a shows the normalized absorbance of the TFSI anion and PC infrared bands plotted as a function of time over three CV cycles from −1 to +1 V. Additionally, the normalized absorbance of the EMIm cation is also plotted as a function of time. At a lower concentration of IL, e.g., Figure 4, the absorbance of the cation could not be detected with accuracy. Interestingly, the results at a higher IL concentration differ from those at the lower IL concentration (Figure 4), where, in addition to the cation and anion of the IL entering and exiting the pores of the CDC upon charging and discharging, the PC also enters and exits the pores in unison with the IL electrolyte. These data suggest that PC entering and exiting CDC pores is IL concentration dependent, where higher IL concentrations can facilitate PC pore transport due to IL−PC solvation interactions.

■ CONCLUSIONS

In conclusion, the ion dynamics of EMIm-TFSI in electrodes made of porous CDCs and nonporous OLCs were investigated on a molecular level and in real time on fully functioning EDLCs with a new in situ infrared spectroelectrochemical technique. These results provide direct evidence of cations and anions of EMIm-TFSI entering and exiting CDC pores during charging and discharging. The results also provide direct evidence that nonporous OLC electrodes store EMIm-TFSI ions on their surface, allowing for rapid charging and discharging with only a small change in concentration in the bulk electrode. When a mixture of IL and organic solvent was used as an electrolyte in the CDC electrodes, the ability of the organic solvent to enter and exit the CDC pores upon charging and discharging was IL concentration dependent.

■ EXPERIMENTAL SECTION

Materials Characterization. The specific surface area and porosity of CDCs and OLCs were determined via gas sorption using a Quadrasorb (Quantachrome Instruments) system. Isotherms were collected at 77 K using N_2 adsorbate. The BET specific surface area (SSA) was calculated for P_0 values in the 0.05−0.10 range,[34] and density functional theory based evaluations of the SSA, pore volume, and pore size distributions were made using quenched solid density functional theory (QSDFT).[35] Quantachrome's Quadrawin software was used for all calculations.

EDLC Fabrication. CDC nanopowders were synthesized from 30 nm diameter titanium carbide particles (>99% purity, PlasmaChem) using a previously described process.[36] A quartz boat containing the material was heated in a quartz furnace to 600 °C under constant Ar flow, exposed to Cl_2 gas at that temperature for 5 h, and annealed in H_2 for 3 h. The resulting material was dried under vacuum (0.001 Torr) at 80 °C for 24 h. OLC particles were produced by placing 5 nm UD-90 nanodiamond particles (NanoBlox Inc.) in a vacuum furnace (Solar Atmospheres) and annealing at 1800 °C for 3 h under 10^{-6}

Torr of pressure.[37] To fabricate test electrodes, the resulting carbon materials were mixed with PTFE fibers (Sigma-Aldrich, 60 wt % dispersion in H_2O) in ethanol at 50 °C in a 9:1 mass ratio. The slurry was rolled into 75 μm thick freestanding films using a 5.5 mg/cm^2 mass loading. The films were cut into 10 mm × 20 mm rectangular sections and were weighed individually, with the average mass equal to 11 mg. The films were placed in an Ar-containing glovebox (Vacuum Atmospheres, <5 ppm of O_2 present). Neat EMIm-TFSI (Boulder Ionics) was added to each electrode in a dropwise fashion, and the electrode was soaked in the electrolyte for 12 h. To prepare the solvated IL/solvent system, PC (Fisher Scientific) and EMIm-TFSI were mixed in a 9:1 or 1:1 mass ratio and stirred together. The resulting solution was added to the electrodes and soaked into the material for 1 h. Excess electrolyte was removed from the electrode surfaces, and 50 nm thick gold foil was pressed on one surface of each film. The films were subsequently compressed into a symmetrical sandwich cell with a layer of separator (Celgard 3501) in between.

Spectroelectrochemical Experiments. A rectangular EDLC with dimensions of 5 × 15 mm was clamped onto the surface of a diamond ATR crystal with a surface area of 3.42 mm^2 using the anvil from the Golden Gate accessory (Specac Inc.) at a constant load capacity of 36 kg. After clamping, the EDLCs with pure EMIm-TFSI electrolyte were allowed to equilibrate for 12 h before voltage was applied, and the EDLCs with a PC/EMIm-TFSI mixture were equilibrated for 1 h to minimize the effect of solvent evaporation. All experiments were performed in a dry chamber, which was purged with moisture-free and CO_2-free air; the kinetics of relative humidity in the chamber after closing the chamber were reported previously[16] (relative humidity decreases to a final value of 0.25%). A Fourier transform infrared (FTIR) spectrometer (Nicolet 6700 series, Thermo Electron Corp.) was used to collect all spectra using a single-reflection diamond ATR Golden Gate accessory. All infrared spectra were collected using a liquid nitrogen-cooled mercury—cadmium—telluride detector at four scans per spectrum and a resolution of 4 cm^{-1}, resulting in a spectrum collected every 1.57 s. All spectra were corrected with a background subtraction of the ATR crystal spectrum.

A potentiostat (Solartron SI 1287, Corrware Software) was used to perform CV, voltage step, and galvanostatic cycle experiments. The EDLC was clamped onto the ATR crystal in a two-electrode cell with aluminum contacts. A two-electrode system was used because of the difficulty of inserting a reference electrode into the EDLC, while it was clamped on the ATR crystal, and because Cl^- ions from the AgCl reference electrode reacted with the gold on the EDLC electrodes at voltages above 0.8 V. The electrode in contact with the ATR crystal is the positively charged working electrode for all experiments. In general, CV experiments were performed from −1.5 to +1.5 V at scan rates varying from 5 to 100 mV/s, where one data point was collected every second. Within the voltage range explored in this study, no evidence of electrolyte decomposition was observed in either the infrared spectroscopy or cyclic voltammetry results. A minimum of three voltage sweeps were performed at each scan rate to ensure the reproducibility of the infrared spectra and CV data. Galvanic cycles were performed by holding the current steady at ±0.001 A while allowing the voltage to vary from −1.5 to +1.5 V.

ASSOCIATED CONTENT

Supporting Information

Calculations and description of the control experiments. This material is available free of charge via the Internet at http://pubs.acs.org.

AUTHOR INFORMATION

Corresponding Author

elabd@drexel.edu

Notes

The authors declare no competing financial interest.

ACKNOWLEDGMENTS

This material is based upon work supported by, or in part by, the U.S. Army Research Laboratory and the U.S. Army Research Office under Contract/Grant W911NF-10-1-0255 and the National Science Foundation under Grant CNS-0960061.

REFERENCES

(1) Miller, J. R.; Simon, P. *Science* **2008**, *321*, 651.
(2) Armand, M.; Endres, F.; MacFarlane, D. R.; Ohno, H.; Scrosati, B. *Nat. Mater.* **2009**, *8*, 621.
(3) Lin, R. Y.; Taberna, P. L.; Fantini, S.; Presser, V.; Perez, C. R.; Malbosc, F.; Rupesinghe, N. L.; Teo, K. B. K.; Gogotsi, Y.; Simon, P. *J. Phys. Chem. Lett.* **2011**, *2*, 2396.
(4) Bazant, M. Z.; Storey, B. D.; Kornyshev, A. A. *Phys. Rev. Lett.* **2011**, *106*, 046102.
(5) Weingaertner, H. *Angew. Chem., Int. Ed.* **2008**, *47*, 654.
(6) Simon, P.; Gogotsi, Y. *Nat. Mater.* **2008**, *7*, 845.
(7) Laudisio, G.; Dash, R. K.; Singer, J. P.; Yushin, G.; Gogotsi, Y.; Fischer, J. E. *Langmuir* **2006**, *22*, 8945.
(8) Kondrat, S.; Georgi, N.; Fedorov, M. V.; Kornyshev, A. A. *Phys. Chem. Chem. Phys.* **2011**, *13*, 11359.
(9) Kondrat, S.; Perez, C. R.; Presser, V.; Gogotsi, Y.; Kornyshev, A. A. *Energy Environ. Sci.* **2012**, *5*, 6474.
(10) Pech, D.; Brunet, M.; Durou, H.; Huang, P. H.; Mochalin, V.; Gogotsi, Y.; Taberna, P. L.; Simon, P. *Nat. Nanotechnol.* **2010**, *5*, 651.
(11) Huang, J. S.; Sumpter, B. G.; Meunier, V.; Yushin, G.; Portet, C.; Gogotsi, Y. *J. Mater. Res.* **2010**, *25*, 1525.
(12) Merlet, C.; Rotenberg, B.; Madden, P. A.; Taberna, P. L.; Simon, P.; Gogotsi, Y.; Salanne, M. *Nat. Mater.* **2012**, *11*, 306.
(13) Wang, H.; Koster, T. K. J.; Trease, N. M.; Segalini, J.; Taberna, P. L.; Simon, P.; Gogotsi, Y.; Grey, C. P. *J. Am. Chem. Soc.* **2011**, *133*, 19270.
(14) Levi, M. D.; Salitra, G.; Levy, N.; Aurbach, D.; Maier, J. *Nat. Mater.* **2009**, *8*, 872.
(15) Levi, M. D.; Levy, N.; Sigalov, S.; Salitra, G.; Aurbach, D.; Maier, J. *J. Am. Chem. Soc.* **2010**, *132*, 13220.
(16) Richey, F. W.; Elabd, Y. A. *J. Phys. Chem. Lett.* **2012**, *3*, 3297.
(17) Li, J. T.; Zhou, Z. Y.; Broadwell, I.; Sun, S. G. *Acc. Chem. Res.* **2012**, *45*, 485.
(18) Osawa, M.; Yoshii, K. *Appl. Spectrosc.* **1997**, *51*, 512.
(19) Kunimatsu, K.; Yoda, T.; Tryk, D. A.; Uchida, H.; Watanabe, M. *Phys. Chem. Chem. Phys.* **2010**, *12*, 621.
(20) Zhang, H. X.; Wang, S. H.; Jiang, K.; Andre, T.; Cai, W. B. *J. Power Sources* **2012**, *199*, 165.
(21) Ohman, M.; Persson, D.; Leygraf, C. *Prog. Org. Coat.* **2006**, *57*, 78.
(22) Hansen, W. N.; Kuwana, T.; Osteryoung, R. A. *Anal. Chem.* **1966**, *38*, 1810.
(23) Largeot, C.; Portet, C.; Chmiola, J.; Taberna, P. L.; Gogotsi, Y.; Simon, P. *J. Am. Chem. Soc.* **2008**, *130*, 2730.
(24) Liu, S.; Liu, W. J.; Liu, Y.; Lin, J. H.; Zhou, X.; Janik, M. J.; Colby, R. H.; Zhang, Q. M. *Polym. Int.* **2010**, *59*, 321.
(25) Richey, F. W.; Elabd, Y. A. *J. Electrochem. Soc.* **2013**, *160*, A862.
(26) Zuleta, M.; Bjornbom, P.; Lundblad, A. *J. Electrochem. Soc.* **2006**, *153*, A48.
(27) Zuleta, M.; Bjornbom, P.; Lundblad, A.; Nurk, G.; Kasuk, H.; Lust, E. *J. Electroanal. Chem.* **2006**, *586*, 247.
(28) Tokuda, H.; Hayamizu, K.; Ishii, K.; Susan, M.; Watanabe, M. *J. Phys. Chem. B* **2005**, *109*, 6103.
(29) Hantel, M. M.; Presser, V.; Kotz, R.; Gogotsi, Y. *Electrochem. Commun.* **2011**, *13*, 1221.
(30) Hantel, M. M.; Presser, V.; McDonough, J. K.; Feng, G.; Cummings, P. T.; Gogotsi, Y.; Kotz, R. *J. Electrochem. Soc.* **2012**, *159*, A1897.
(31) Tsai, W.-Y.; Lin, R.; Murali, S.; Li Zhang, L.; McDonough, J. K.; Ruoff, R. S.; Taberna, P.-L.; Gogotsi, Y.; Simon, P. *Nano Energy* **2013**, *2*, 403.

(32) Gebbie, M. A.; Valtiner, M.; Banquy, X.; Fox, E. T.; Henderson, W. A.; Israelachvili, J. N. *Proc. Natl. Acad. Sci. U.S.A.* **2013**, *110*, 9674.
(33) Lin, R.; Huang, P.; Segalini, J.; Largeot, C.; Taberna, P. L.; Chmiola, J.; Gogotsi, Y.; Simon, P. *Electrochim. Acta* **2009**, *54*, 7025.
(34) Brunauer, S.; Emmett, P. H.; Teller, E. *J. Am. Chem. Soc.* **1938**, *50*, 309.
(35) Gor, G. Y.; Thommes, M.; Cychosz, K. A.; Neimark, A. V. *Carbon* **2012**, *50*, 1583.
(36) Perez, C. R.; Yeon, S. H.; Segalini, J.; Presser, V.; Taberna, P. L.; Simon, P.; Gogotsi, Y. *Adv. Funct. Mater.* **2013**, *23*, 1081.
(37) McDonough, J. K.; Frolov, A. I.; Presser, V.; Niu, J. J.; Miller, C. H.; Ubieto, T.; Fedorov, M. V.; Gogotsi, Y. *Carbon* **2012**, *50*, 3298.